

---

Title	Non-stoichiometric FePt nanoclusters for heated dot magnetic recording media
Author(s)	John Rex Mohan, Rohit Medwal, Surbhi Gupta, Kriti Gogia, Joseph Vimal Vas, Rekha Gupta, Angshuman Deka, Rajdeep Singh Rawat, Annapoorni Subramanian, and Yasuhiro Fukuma

---

Copyright © 2021 American Chemical Society

This is an Accepted Manuscript of an article published by American Chemical Society in *ACS Applied Nano Materials* on 13/07/2021, available online:  
<https://doi.org/10.1021/acsnm.1c01085>

# Non-stoichiometric FePt nanoclusters for Heated Dot Magnetic Recording Media

John Rex Mohan<sup>1#</sup>, Rohit Medwal<sup>2, #, \*</sup>, Surbhi Gupta<sup>1, 2</sup>, Kriti Gogia<sup>3</sup>, Joseph Vimal Vas<sup>2</sup>, Rekha Gupta<sup>4</sup>, Angshuman Deka<sup>1</sup>, Rajdeep Singh Rawat<sup>2</sup>, Subramanian Annapoorni<sup>4</sup>, and Yasuhiro Fukuma<sup>1\*</sup>

<sup>1</sup>*School of Computer Science and System Engineering, Kyushu Institute of Technology, Iizuka, Fukuoka 820-8502, Japan.*

<sup>2</sup>*Natural Science and Science Education, National Institute of Education, Nanyang Technological University, 637616, Singapore.*

<sup>3</sup>*Department of Emergency Medicine, Weill Cornell Medicine, New York, NY 10065, United States*

<sup>4</sup>*Department of Physics and Astrophysics, University of Delhi, Delhi, 110007, India.*

# Contributed equally

Correspondence: \*[rohit.medwal@nie.edu.sg](mailto:rohit.medwal@nie.edu.sg), \*[fukuma@cse.kyutech.ac.jp](mailto:fukuma@cse.kyutech.ac.jp)

## Abstract

Heated-dot-magnetic-recording (HDMR) provides a path to increase the areal density of magnetic recording media beyond 4 Tb/in<sup>2</sup>. HDMR based recording media requires ultra-small, non-interacting and thermally stable magnetic dots with high perpendicular anisotropy. We have synthesized non-stoichiometric Fe<sub>60</sub>Pt<sub>40</sub> nanoclusters with and without Pt buffer layer on silicon substrates, which shows a reduction in chemical ordering temperature. The Fe<sub>60</sub>Pt<sub>40</sub> nanoclusters retain the hard-magnetic phase up to 1023 K with the coercive field of 1.3 Tesla due to the Pt element compensation from the buffer layer. This compensation of Pt was confirmed through XRD investigations where two distinct phases of Fe<sub>3</sub>Pt, and FePt<sub>3</sub> are observed at elevated annealing temperature. Micromagnetic simulations were performed to understand the effect of magnetic-anisotropy, dipolar interaction and exchange-coupling between the soft magnetic Fe<sub>3</sub>Pt and hard magnetic FePt. The results imply that non-stoichiometric Fe<sub>60</sub>Pt<sub>40</sub> with Pt buffer layer facilitates low chemical ordering temperature retaining the high perpendicular anisotropy with minimal non-interacting behavior, suitable for HDMR.

**Keywords** - *Information storage, Heated dot magnetic recording, FePt, non-stoichiometric, magnetization reversal.*

## I. Introduction

Successful implementation of Heated Dot Magnetic Recording (HD MR) technology enables the increase in areal density of magnetic recording media beyond the achieved 4 Tb/in<sup>2</sup><sup>1-3</sup>. To realize HD MR, media materials with high magneto-crystalline anisotropy such as FePt and CoPt are best suited due to their high uniaxial anisotropy ( $K_u \geq 10^6 \text{ J m}^{-3}$ )<sup>2,4</sup>. In film based granular media,  $L1_0$  FePtC, (FePt)Ag-C, exchange coupled CoPt/FePt, Fe/FePt, FePt/FeRh, FePt:C/Fe are widely investigated for tuning the switching field distribution and thermal stability<sup>25-31</sup>. The high  $K_u$  of FePt and CoPt would also require a high magnetization switching field for write operations, which can be temporarily reduced by localized laser heating. The laser locally heats the isolated bit of the recording media to momentarily reduce the  $K_u$  before recording the information<sup>5</sup> assisted by a near-field-transducer element. Despite these advancements, the critical challenge during this high-temperature writing is the thermal stability of the selected pattern and its magnetic interaction with neighboring bits which requires further optimization<sup>2,6</sup>.

Self-assembled FePt nanoparticles (NPs) are widely studied for developing the bit-per-grain pattern media<sup>5</sup>. The as-prepared FePt NPs exhibit disordered A1 i.e. face-centered cubic (FCC) phase and require subsequent thermal treatment above  $\sim 780 \text{ K}$  to transform into  $L1_0$  face-centered tetragonal (FCT) phase which display high  $K_u$ , required for designing of thermally stable recording media<sup>7-9</sup>. Surfactants such as oleylamine and oleic acid are commonly used for synthesising these NPs to ensure the uniform size distribution and reduced magnetic interaction among them, also facilitating self-organization. The organic coating results in a carbonaceous layer around the nanoclusters (NCs) after thermal annealing, which allows the clusters to be self-stabilized against natural oxidation<sup>3,10-12</sup>. However, high annealing temperature leads to particle sintering, size increase, and agglomeration<sup>13-15</sup>. Alternatively, this indispensable sintering growth

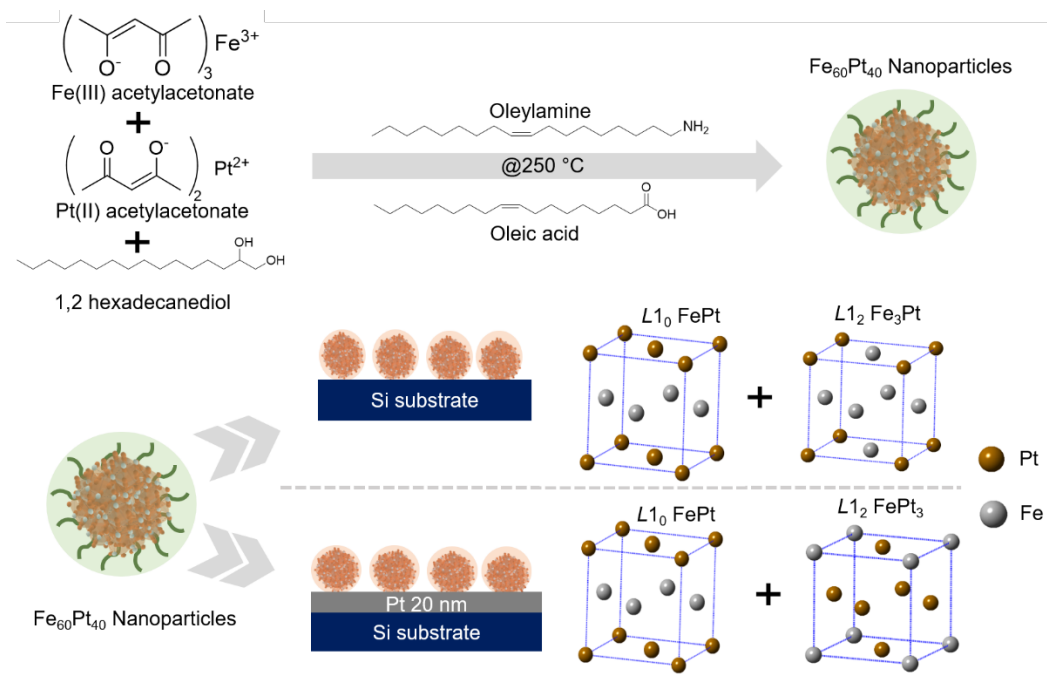
of NPs can be controlled by reducing this ordering temperature of FCT phase by doping of materials such as Ag, NaCl, Pb, Bi, which modifies the grain growth kinetics<sup>16-18</sup>. For instance, Pb doping reduces the ordering kinetics and Bi doping allows for a slower diffusion which provides superior surface segregation of dopants even at low temperature annealing. The ordering temperature can also be reduced by varying the relative composition of Fe and Pt in the FePt alloy system<sup>19-22</sup>. Such a variation in the elemental composition of Fe and Pt in the alloy provides controlled particle size distribution but may affect the magnetic properties including the magnetic anisotropy and the saturation magnetization. The chemical synthesis route provides a superior controllability in achieving a high performance HDMR media. Choosing the composition of metal precursors for the synthesis process requires careful attention<sup>23,24</sup>.

In the present work, non-stoichiometric Fe<sub>60</sub>Pt<sub>40</sub> NPs are synthesized using the chemical co-reduction method and subsequently, two systems 1) Si/Fe<sub>60</sub>Pt<sub>40</sub> and 2) Si/Pt/Fe<sub>60</sub>Pt<sub>40</sub> are investigated in detail. The effect of annealing temperature on chemical ordering in both Si/Fe<sub>60</sub>Pt<sub>40</sub> and Si/Pt/Fe<sub>60</sub>Pt<sub>40</sub> systems were investigated and compared with equi-atomic FePt composition. To understand the effect of magnetocrystalline anisotropy and dipolar exchange contributions of the Si/Fe<sub>60</sub>Pt<sub>40</sub> and Si/Pt/Fe<sub>60</sub>Pt<sub>40</sub> systems, micromagnetic simulations were utilized using commercial LLG Micromagnetic Simulator™. The addition of the platinum buffer layer between Si substrate and Fe<sub>60</sub>Pt<sub>40</sub> NPs is expected to lower the chemical ordering temperature as well as a good thermal stability during the high-temperature processing<sup>32</sup>.

## II. Experimental and characterization methods

A non-stoichiometric amount of Fe(acac)<sub>3</sub> (0.65mmol) and Pt (acac)<sub>2</sub> (0.35 mmol) were mixed in 40 ml phenyl ether with 0.5 mmol Oleic acid, 0.5 mmol Oleylamine and 4 mmol of 1,2 hexadecanediol. This mixture was stirred for 30 min. under inert Argon gas. Thereafter, processing

temperature was increased to 373 K and held for next 30 min. to dissociate the metal precursors into metal ions, followed by refluxing at 523 K for another 30 min<sup>7,33</sup>. The solution was then cooled down to room temperature. Thereafter, 40 ml Ethanol was added followed by 15 min. of stirring. The resultant black precipitate of NPs was washed thoroughly with ethanol and centrifuged at 12000 rpm for 15 min. and finally dispersed in 20 mL Hexane. The dispersed NPs were drop-casted on Si and Si/Pt(20nm) substrates. The deposited NPs assemblies on both substrates were annealed at successive temperatures ( $T_a$ ) from 673 K to 1023 K. A schematic diagram of the process is illustrated in Scheme 1. The annealing was performed using microprocessor-controlled furnace under forming gas (10% Hydrogen and 90% Argon) for 60 min. with a ramp rate of 5 K per minute. Hereafter, we shall discuss these two systems as (1) Si/Fe<sub>60</sub>Pt<sub>40</sub> and (2) Si/Pt/Fe<sub>60</sub>Pt<sub>40</sub>. The first system (Si/Fe<sub>60</sub>Pt<sub>40</sub>) was investigated to compare the effect of non-stoichiometry with equi-atomic ratio system, while the second system (Si/Pt/Fe<sub>60</sub>Pt<sub>40</sub>) was studied to probe the composition compensation effect arising from self-diffusion of Pt into Fe<sub>60</sub>Pt<sub>40</sub> system at high  $T_a$ .



**Scheme 1.** Synthesis and annealing process of non-stoichiometric Fe<sub>60</sub>Pt<sub>40</sub> nanoparticles.

The as-prepared Si/Fe<sub>60</sub>Pt<sub>40</sub> sample was analysed using Rutherford backscattering (RBS) with a 2 MeV particle beam to estimate the elemental composition. A Tecnai T30 and JEOL ARM 300F GrandARM Transmission Electron Microscopes (TEM) were used to study the size and shape of the NPs dispersed on the carbon-coated copper grid. X-ray diffraction (XRD) data in the 2θ range 20°–55° were collected using a Bruker (D8) diffractometer. The software TOPAS was used to perform Rietveld refinement to identify crystallographic phases. Vibrating Sample Magnetometer (VSM) Micro Sense EV9 with a maximum field of ±2.2 T was used for recording the room temperature out-of-plane M-H hysteresis curve. Air-cooled argon-ion laser Raman spectrometer from Renishaw (Invia) was used to record the Raman spectra from 0-3000 cm<sup>-1</sup> range to detect carbonaceous layer properties.

### III. Results and discussion

Figure 1(i) shows the recorded RBS spectrum of as-prepared Si/Fe<sub>60</sub>Pt<sub>40</sub>. The black dots represent the experimental data while the red line represents the simulated spectrum using the Rutherford Universal Manipulation Program simulation code. The elemental composition of the sample is estimated to be Fe, 60% and Pt, 40%. Note that the composition was controlled by optimizing precursors in our previous study<sup>15</sup>, where 1:1 ratio of metal precursors resulted in near to stoichiometric composition of Fe<sub>46</sub>Pt<sub>54</sub>. The synthesized NPs are subjected to TEM studies and clearly reveal the formation of hexagonal closed packed self-organization of monodispersed Fe<sub>60</sub>Pt<sub>40</sub> NPs as shown in Fig. 1(iii). The observed hexagonal packing is achieved by optimizing the Oleic acid and Oleylamine ratio as surfactants during synthesis, which establishes a protective layer around NPs and prevents them from approaching each other. The average particle size of the NPs is estimated to be ~2 nm using the ImageJ software. Figure. 1(iii-vi) show the TEM images

of successively annealed NPs at  $T_a = 623\text{K}$ ,  $823\text{K}$  and  $1023\text{K}$ . The average particle size increases up to  $\sim 11\text{ nm}$  after highest temperature treatment of  $1023\text{K}$ . The formation of a carbonaceous overcoat due to the outgassing of hydrogen from surfactants at higher annealing temperature is confirmed by the Raman spectra as shown in Fig. 1(ii). From the Raman spectra, the characteristic peak at  $1350\text{ cm}^{-1}$  confirms the presence of disordered carbon, marked as “D” whereas the peak at  $1590\text{ cm}^{-1}$  is due to graphitic carbon formation and marked as “G”. The carbonaceous layer provides two-fold advantages which are controlling the size of NPs and enabling self-stabilization by preventing unwanted natural oxidation.

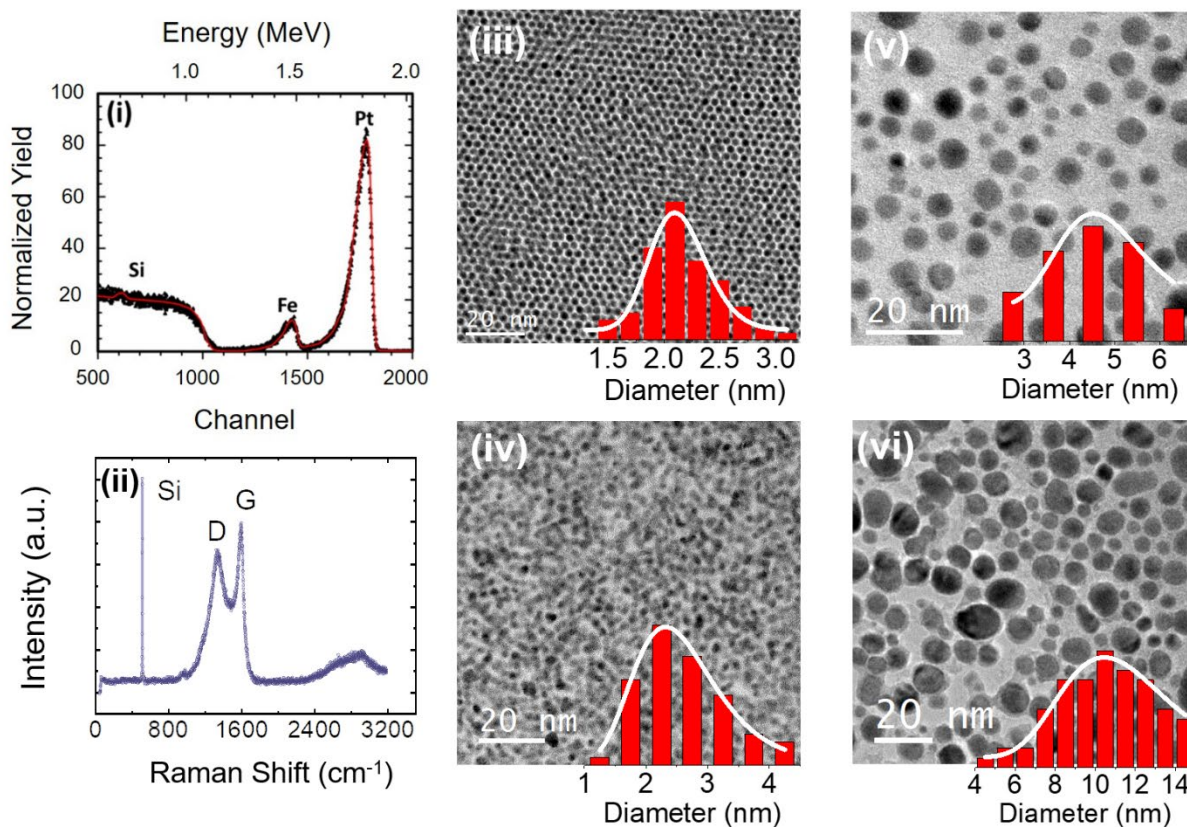


**Figure 1.** (i) RBS spectra of as-prepared  $\text{Fe}_{60}\text{Pt}_{40}$  NPs, (ii) Raman spectra of  $1023\text{ K}$  annealed NPs, TEM images of (iii) as-prepared  $\text{Fe}_{60}\text{Pt}_{40}$  NPs, (iv) TEM image of  $673\text{ K}$  annealed NPs, (v) TEM image of  $873\text{ K}$  annealed NPs, (vi) TEM image of  $1023\text{ K}$  annealed NPs.

The XRD patterns of as-prepared and annealed Si/Fe<sub>60</sub>Pt<sub>40</sub> and Si/Pt/Fe<sub>60</sub>Pt<sub>40</sub> samples at different T<sub>a</sub> are shown in Fig. 2(i) and (ii) respectively. The XRD pattern of the as-prepared Si/Fe<sub>60</sub>Pt<sub>40</sub> sample shows a hump centered at 2θ = 40.17° corresponding to (111) plane of FePt and attributes to the disordered A1 phase. Annealing at T<sub>a</sub> = 773 K results in a hump at 47.43° corresponding to (200) reflection. At T<sub>a</sub> = 873 K, the emergence of superlattice peaks corresponding to (001) and (110) planes with sharp intensities at 24.13° and 33.04° respectively, provides a clear evidence of the evolution of chemical ordering in the sample. The thermal energy induced superlattice peaks are a characteristic feature of chemical ordering attributed to the alternative stacking of Fe and Pt atomic planes in the FePt unit cell. A preferred (001) orientation is observed in Si/Fe<sub>60</sub>Pt<sub>40</sub>, which was not observed for the equi-atomic FePt in our earlier report<sup>33</sup>. In addition, a split in the (200) peak into (200) and (002) peaks at 2θ = 47.36° and 49.23° respectively, reveals the induced tetragonality in the unit cell because of chemical ordering. The corresponding lattice distortion *c/a* value of the sample annealed at 873 K is estimated to be ~ 0.964, indicating the degree of asymmetry in the FePt unit cell and further confirming the phase transformation from cubic to tetragonal phase. On further increase of T<sub>a</sub> to 973 K, the relative intensity of (001) with respect to (111) peak decreases and the additional shoulder starts to appear adjacent to (111) peak resulting in asymmetry corresponding to a mixed FePt phase. At T<sub>a</sub> = 1023 K, the shoulder at (111) peak becomes distinct with enhanced intensity, confirming the presence of an additional phase identified as Fe<sub>3</sub>Pt phase (marked by \*). The XRD study clearly reveals the temperature dependent structural phase transformation from A1 (Fm3m) to L<sub>10</sub> (P4/mmm) phase and then to a mixed phase of L<sub>10</sub> and L<sub>12</sub> (Pm3m).

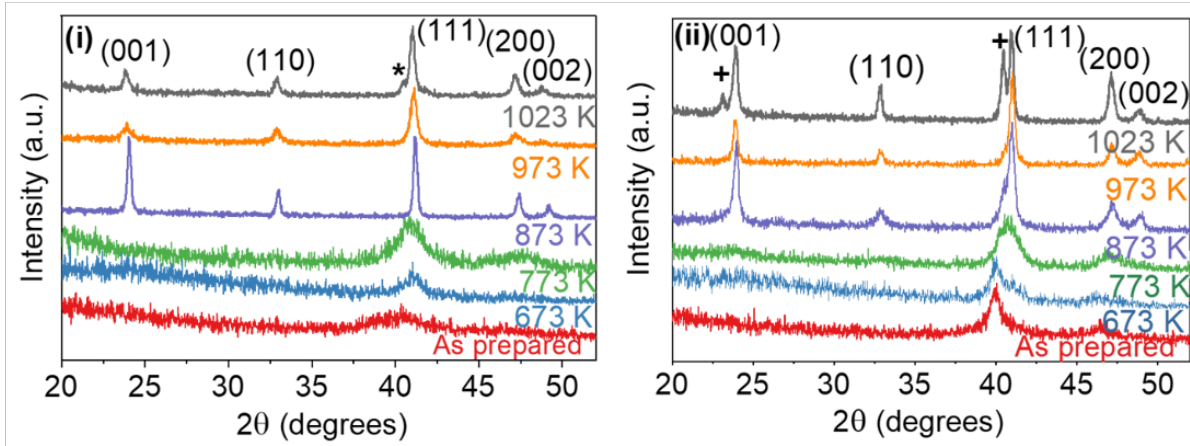


**Figure 2.** XRD patterns of (i) Si/Fe<sub>60</sub>Pt<sub>40</sub> and (ii) Si/Pt/Fe<sub>60</sub>Pt<sub>40</sub> system annealed at  $T_a$  from 673 K to 1023 K.

The XRD patterns of Si/Pt/Fe<sub>60</sub>Pt<sub>40</sub> show a similar behavior for as-prepared and  $T_a = 673$  K annealed samples. However, after  $T_a = 773$  K processing, a clear shift in peak at  $2\theta = 41.25^\circ$  related to (111) peak and the presence of broaden hump at  $2\theta = 46.46^\circ$  corresponds to the A1 phase appears. Also, onset of additional (001) and (110) peaks dictate the partial transformation into  $L_{10}$  FePt at relatively lower  $T_a$  of 773 K with an additional FePt<sub>3</sub>. On further increase of  $T_a$  to 873 K, characteristics split of (200) peak at  $2\theta = 47.36^\circ$  and  $49.23^\circ$  correspondingly to (200) and (002) respectively confirms the induced tetragonality in the unit cell due to chemical ordering. On the other hand, at  $T_a = 973$  K, asymmetry in (111) peak becomes more prominent, providing evidence of the presence of a mixed phase. At  $T_a = 1023$  K, this asymmetric peak splits into two distinct peaks at  $2\theta = 40.41^\circ$  and  $41.03^\circ$  corresponding to (111) of chemically ordered  $L_{12}$  FePt<sub>3</sub> phase (indicated by +) and chemically ordered  $L_{10}$  FePt phase. Interestingly, for Si/Pt/Fe<sub>60</sub>Pt<sub>40</sub>, the preferred orientation along (001) reflection is retained up to  $T_a = 1023$  K; hence it is evident that

the Pt buffer layer is promoting the preferred orientation in Si/Pt/Fe<sub>60</sub>Pt<sub>40</sub> in addition to lowering the ordering temperature compared to Si/Fe<sub>60</sub>Pt<sub>40</sub>.

Further to quantify respectively the Fe<sub>3</sub>Pt and FePt<sub>3</sub> phase, Rietveld fitting of XRD patterns for Si/Fe<sub>60</sub>Pt<sub>40</sub> and Si/Pt/Fe<sub>60</sub>Pt<sub>40</sub> annealed at 1023 K are performed. Figures 3(i) and (ii) show the experimental and Rietveld refined patterns (de-convoluted) of Si/Fe<sub>60</sub>Pt<sub>40</sub>. Figure 3 (i) shows the simulated XRD pattern corresponds to the *L*<sub>10</sub> FePt phase. All the observed peaks in the XRD patterns are indexed with the P4/mmm space group. Figure 3(ii) shows the XRD pattern corresponding to the *L*<sub>12</sub> Fe<sub>3</sub>Pt phase and indexed with space group Pm3m. The lattice parameter corresponding to cubic *L*<sub>12</sub> Fe<sub>3</sub>Pt unit cell was estimated to be 3.82 Å and, for tetragonal *L*<sub>10</sub> FePt phase, lattice parameters **a** = 3.85 Å and **c** = 3.73 Å. A similar exercise was also performed for the XRD pattern obtained for Si/Pt/Fe<sub>60</sub>Pt<sub>40</sub>. In this case, two phases corresponding to FePt and FePt<sub>3</sub> were considered during Rietveld refinement fitting. The experimentally observed and the de-convoluted XRD patterns corresponding to *L*<sub>10</sub> FePt and *L*<sub>12</sub> FePt<sub>3</sub> phases are given in Fig. 4 (i) and (ii) respectively. The lattice parameter for *L*<sub>12</sub> FePt<sub>3</sub> was estimated to be **a** = 3.86 Å and for the *L*<sub>10</sub> FePt phase, lattice constant **a** = 3.86 Å and **c** = 3.73 Å. Hence, Rietveld analysis clearly shows the evidence of an additional phase corresponding to FePt<sub>3</sub>, which may be due to the diffusion of platinum from the buffer layer in the annealing process.

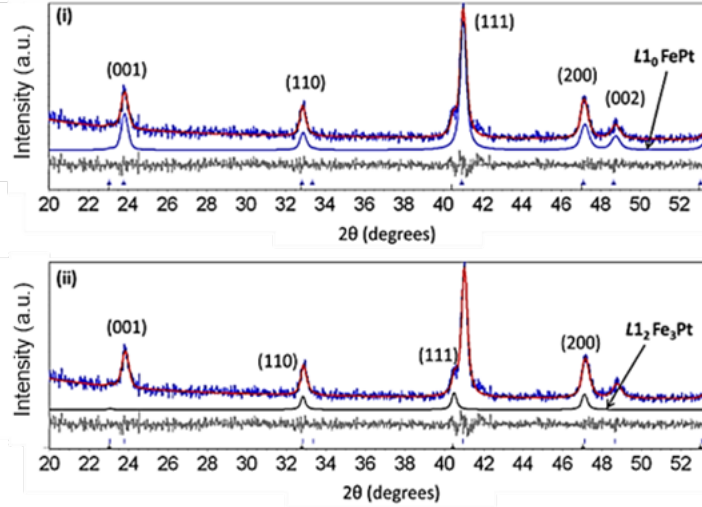


**Figure 3.** Deconvolution to (i) FCT  $L1_0$ -FePt phase and (ii) FCC  $L1_2$ -Fe<sub>3</sub>Pt phase in experimentally obtained XRD pattern of 1023 K annealed Si/Fe<sub>60</sub>Pt<sub>40</sub> system.

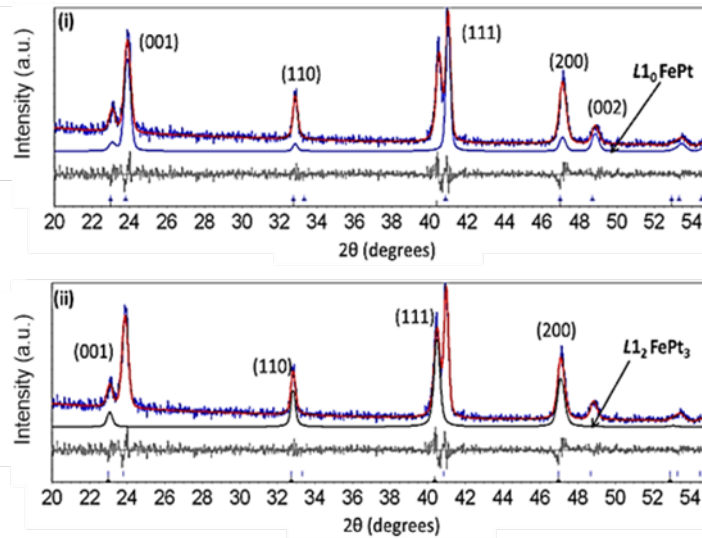


**Figure 4.** Deconvolution to (i) FCT  $L1_0$ -FePt and (ii) FCC  $L1_2$ -FePt<sub>3</sub> phase in experimentally obtained XRD pattern of 1023 K annealed Si/Pt/Fe<sub>60</sub>Pt<sub>40</sub> system.

Figures. 5(i) and (ii) show the normalized M-H hysteresis behavior of as-prepared and annealed Si/Fe<sub>60</sub>Pt<sub>40</sub> and Si/Pt/Fe<sub>60</sub>Pt<sub>40</sub> samples. All M-H curves are recorded at room temperature in out-of-plane geometry. The as-prepared Si/Fe<sub>60</sub>Pt<sub>40</sub> sample exhibits neither a square curve nor a tendency to saturate up to H = 2 T. The sample annealed at T<sub>a</sub> = 673 K exhibited only small

coercive field  $\mu_0 H_c$  of 0.03 T. The value of  $\mu_0 H_c$  increases from 0.23 T for  $T_a = 773$  K to 1.17 T for  $T_a = 873$  K. On the other hand, equi-atomic FePt attained lower  $\mu_0 H_c \sim 0.58$  T after  $T_a = 873$  K, which is reported earlier<sup>15</sup>. Hence, the deviation from equi-atomic stoichiometry promotes the chemical ordering at relatively low  $T_a = 773$  K compared to  $T_a = 873$  K processing. In Fig. 5(i), the presence of a small shoulder near low magnetic field indicates the existence of soft magnetic Fe<sub>3</sub>Pt phase, which is also evident from XRD studies. Further improvement in the coercivity  $\mu_0 H_c = 1.33$  T is obtained for  $T_a = 973$  K. However, for  $T_a = 1023$  K, a decrease in the coercivity to 0.60 T with a pinched curve shows a decoupled behavior of soft and hard magnetic phases. For Si/Pt/Fe<sub>60</sub>Pt<sub>40</sub>, the as-prepared sample shows a soft magnetic behavior, similar to as-prepared Si/Fe<sub>60</sub>Pt<sub>40</sub>. However, the sample annealed at  $T_a = 673$  K, shows higher value of  $\mu_0 H_c \sim 0.12$  T as compared to  $\mu_0 H_c \sim 0.03$  T for Si/Fe<sub>60</sub>Pt<sub>40</sub>, which further increases to 0.23 T after  $T_a = 773$  K process. For  $T_a = 873$  K, a sudden rise of  $\mu_0 H_c \sim 1.24$  T confirms the formation of hard magnetic FePt *L*<sub>10</sub> phase. The shoulder near the low magnetic field is due to the existence of the FePt<sub>3</sub> phase. For  $T_a = 973$  K, a slight reduction in the coercivity can be observed. This reduction is due to the exchange spring composite behavior of magnetically hard *L*<sub>10</sub> FePt phase and magnetically soft *L*<sub>12</sub> FePt<sub>3</sub> phase. However, with further annealing at 1023 K, the sample retains such high value of coercivity and shows a stability in the magnetic hardness. This observed stability is attributed to the diffusion of Pt atoms to Fe rich FePt. The variation of coercivity for the Fe<sub>60</sub>Pt<sub>40</sub> samples and Fe<sub>46</sub>Pt<sub>54</sub><sup>15</sup> is plotted in Fig. 5(iii). The coercivity of Fe<sub>46</sub>Pt<sub>54</sub> monotonically increases with  $T_a$  up to 1023 K. However, for Si/Fe<sub>60</sub>Pt<sub>40</sub>, the coercivity increases with increasing  $T_a$  up to 973 K and later decreases at  $T_a = 1023$  K. In the case of Si/Pt/Fe<sub>60</sub>Pt<sub>40</sub>, the coercivity increases with an increase of  $T_a$  up to 873 K. Thereafter, the coercivity becomes stable even at high temperature treatment, which is one of the essential requirements to improve the intense laser induced change

in the magnetic properties while writing information in HAMR and HDMR media. The calculated magnetic anisotropy for different annealing temperatures for the Fe<sub>60</sub>Pt<sub>40</sub> samples is shown in Fig.5(iv). The values are calculated based on the relationship  $H_c = 2K_1/\mu_0 M_s$ , where  $\mu_0 M_s = 1.43$  T for bulk FePt NPs is considered. The presence of hard and soft FePt phases within the NPs have been ignored for this formulation.

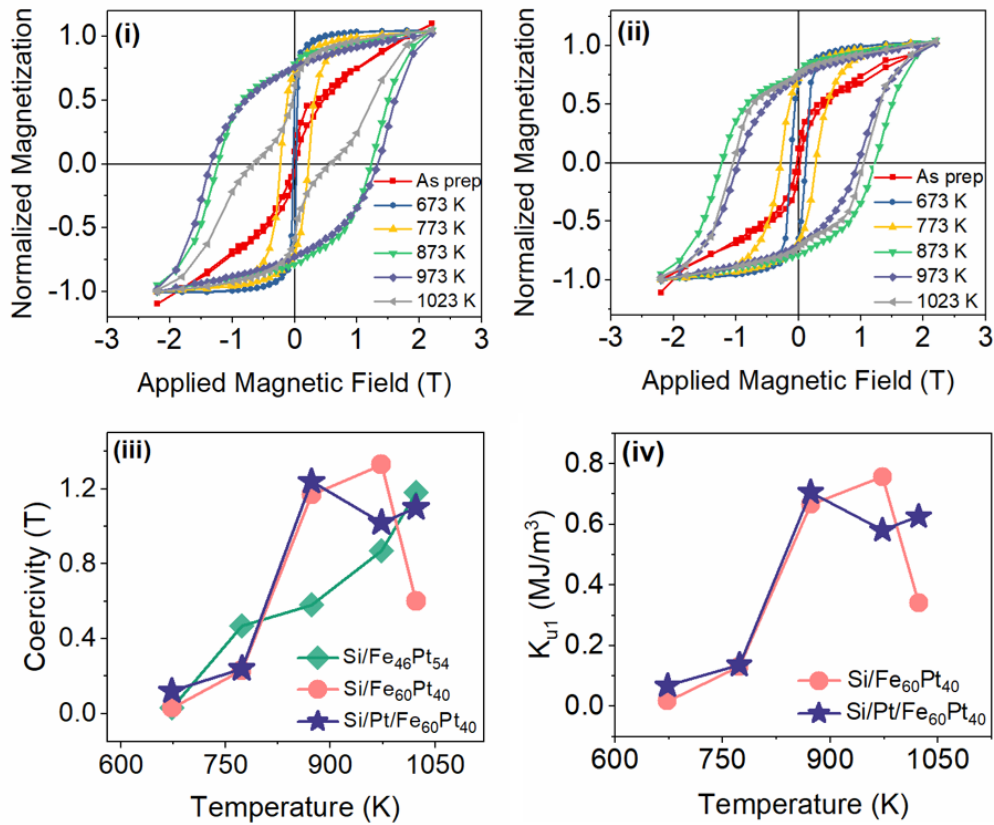


**Figure 5.** Out-of-plane M-H curves of (i) Si/Fe<sub>60</sub>Pt<sub>40</sub> and (ii) Si/Pt/Fe<sub>60</sub>Pt<sub>40</sub> samples at different annealing temperatures. (iii) coercive field as a function of annealing temperature for Si/Fe<sub>60</sub>Pt<sub>40</sub>, Si/Pt/Fe<sub>60</sub>Pt<sub>40</sub> and equiatomic composition<sup>15</sup> (with permission) (iv) Calculated magnetic anisotropy of NPs for different annealing temperature.

Micromagnetic simulations were carried out to gain further insight of interparticle distance relationship with the exchange-coupled soft and hard FePt structures. Owing to the strong

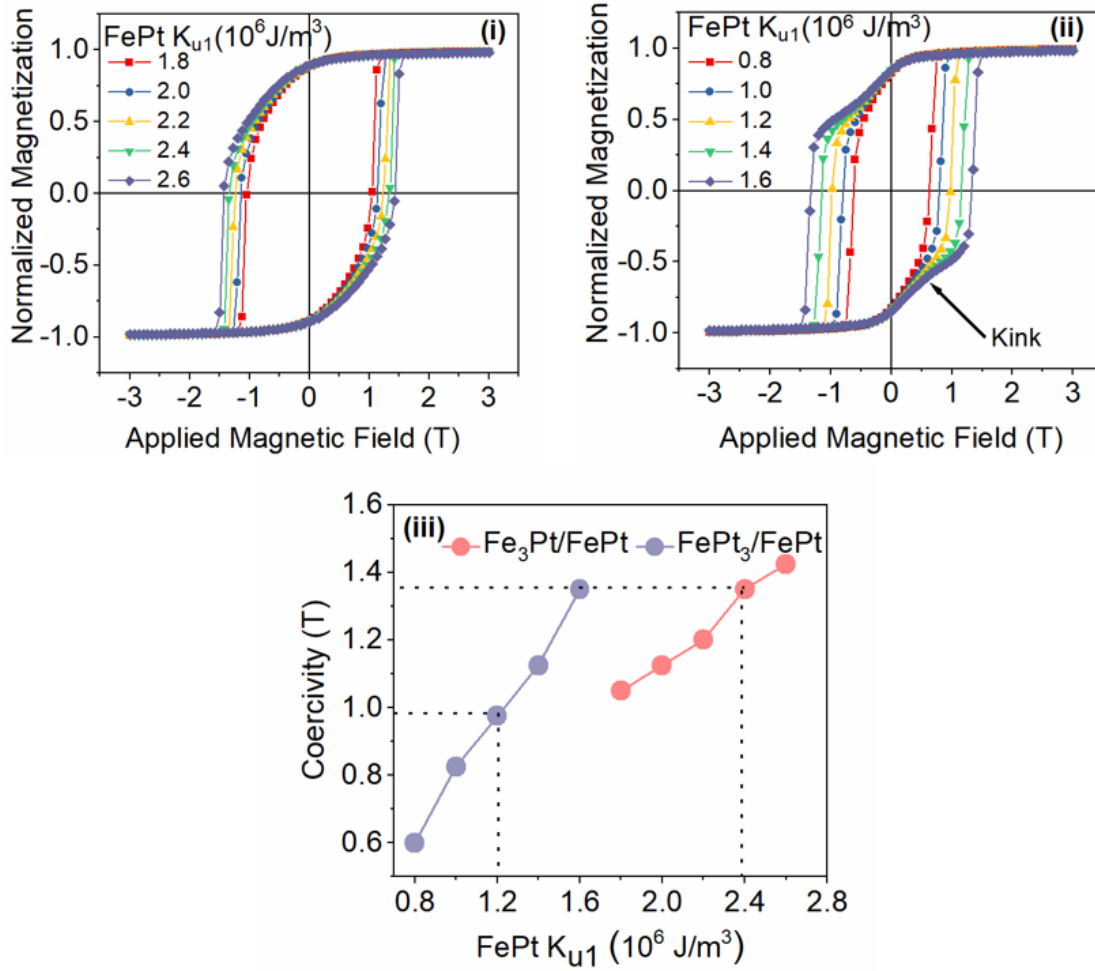
exchange coupling and interaction between the hard and soft layers, exchange spring magnets have added advantages in reducing the coercive field and maintaining the thermal stability. In order to have a meaningful comparison of experimental results and theoretical simulations, we considered the following assumptions. We modeled Si/Fe<sub>60</sub>Pt<sub>40</sub> and Si/Pt/Fe<sub>60</sub>Pt<sub>40</sub> systems as an array of 4×4 cylinder-shaped bits consists of an exchange-coupled Fe<sub>3</sub>Pt/FePt and FePt<sub>3</sub>/FePt bilayers, respectively. Comparing XRD patterns of the samples annealed at 973 K and 1023 K, a clear dissociation of Fe<sub>3</sub>Pt and FePt<sub>3</sub> phases is observed only in 1023 K annealed samples. This indicates that after T<sub>a</sub> = 973 K processing, soft layers are strongly exchanged coupled with the hard FePt layer. Moreover, from the M-H curve of 973 K annealed samples, further confirmation of the exchange coupling behaviour can be seen with the absence of kinks or two-phase reversal. Hence the experimental M-H curves of 973K annealed samples was compared with the simulated curves for analyzing the exchange coupling behavior. The total thickness and diameter of each bit was fixed to 12 nm since TEM analysis of the sample annealed at 1023 K exhibited spherical shaped particles with an average particle size between 11-12 nm. Despite not having any direct thickness measurements of each layer, we assumed the soft layer thickness should be within the exchange length of the hard layer in accordance with the reversal mechanism to be the coherent rotation<sup>34</sup>.

Table 1: Parameters used for the Micromagnetic simulation

Material	Parameter	Value
<b>FePt</b>	$M_s$	$1.14 \times 10^6 \text{ A m}^{-1}$
	$A_{\text{ex}}$	$1.13 \times 10^{-11} \text{ J m}^{-1}$
	$K_{u1}$	$0.8 - 2.6 \times 10^6 \text{ J m}^{-3}$
<b>Fe<sub>3</sub>Pt</b>	$M_s$	$1.43 \times 10^6 \text{ A m}^{-1}$
	$A_{\text{ex}}$	$2.5 \times 10^{-11} \text{ J m}^{-1}$
	$K_{u1}$	$0 \text{ J m}^{-3}$
FePt <sub>3</sub>	$M_s$	$0.56 \times 10^6 \text{ A m}^{-1}$
	$A_{\text{ex}}$	$0 \text{ J m}^{-1}$
	$K_{u1}$	$0 \text{ J m}^{-3}$

We performed set of preliminary simulations with fixed 12 nm thickness, varying the soft layer thickness in an increment of 2 nm, and keeping the magnetic anisotropy of  $K_{u1} = 1.8 \times 10^6 \text{ Jm}^{-3}$ . By mimicking the experimental M-H curves with the simulation, we first optimized the thickness of soft and hard layers to be 4:8 aspect ratio. Each bit was then modeled as a bilayer of 4 nm soft ferromagnetic  $\text{Fe}_3\text{Pt}$  or  $\text{FePt}_3$  bottom layer and 8 nm top hard ferromagnetic  $\text{FePt}$  layer. The simulation parameters are given in table 1. The discretization size for the simulations was chosen to be  $1 \text{ nm} \times 1 \text{ nm} \times 1 \text{ nm}$ . The magnetic easy axes of  $\text{FePt}$  were set to have a minimum orientation along in-plane direction and maximum along out-of-plane direction to imitate the mis-orientation of easy axes in NPs. The easy axes of  $\text{Fe}_3\text{Pt}$  were set in the in-plane direction with cubic anisotropy while for  $\text{FePt}_3$ , the easy axes were adjusted to be equally

oriented in all three directions (33% of X, Y, Z) to mimic a room temperature paramagnetic behavior<sup>35</sup>.



**Figure 6.** Simulated out-of-plane M-H curves (i) Fe<sub>3</sub>Pt/FePt and (ii) FePt<sub>3</sub>/FePt for different FePt magnetocrystalline anisotropies (iii) coercivity as a function of FePt anisotropy.

Figures 6(i) and (ii) show the simulated M-H curves for Fe<sub>3</sub>Pt/FePt and FePt<sub>3</sub>/FePt with different  $K_{u1}$  (FePt). The coercivity increases monotonically with the anisotropy. The reversal mechanisms of both systems confirms the strong exchange spring behavior in such a way that the bilayers reverse together. The  $K_{u1}$  values obtained from the simulation for the corresponding experimental

coercivity values are  $2.4 \times 10^6 \text{ J m}^{-3}$  and  $1.2 \times 10^6 \text{ J m}^{-3}$  for  $\text{Fe}_3\text{Pt/FePt}$  and  $\text{FePt}_3/\text{FePt}$ , respectively. Note that there is a reduction of  $K_{u1}(\text{FePt})$  value in  $\text{FePt}_3/\text{FePt}$  compared to  $\text{Fe}_3\text{Pt/FePt}$ . This is due the variation in the  $M_s$  of the soft layers, for  $\text{FePt}_3/\text{FePt}$ , high  $M_s$  of both layers result in a higher anisotropy than with  $\text{FePt}_3/\text{FePt}$  layers with much lower  $M_s$ <sup>28</sup>. In addition,  $\text{FePt}_3/\text{FePt}$  with higher  $K_{u1}(\text{FePt}) = 1.6 \times 10^6 \text{ J m}^{-3}$  shows a small kink. A similar kink can also be seen in the experimental M-H curve obtained for the  $\text{Si/Pt/Fe}_{60}\text{Pt}_{40}$  sample annealed at  $T_a = 1023 \text{ K}$  in Fig. 5(ii), indicating a decoupled behavior in the bilayer. Although there is no variation in the interlayer exchange coupling, an increase of  $K_{u1}(\text{FePt})$  leads to magnetic decoupling. This reduction of anisotropy can be attributed to the formation of graded interface as reported earlier<sup>34,37</sup> and would require a more detailed study. In either case, the presence of exchange spring behavior in  $\text{Si/Pt/Fe}_{60}\text{Pt}_{40}$  is considered to be responsible for the reduction of  $K_{u1}(\text{FePt})$  which would be beneficial for lowering the writing temperature. In addition, the decoupled behavior with higher  $K_{u1}(\text{FePt})$  indicates that even for  $\text{Si/Pt/Fe}_{60}\text{Pt}_{40}$  sample annealed at  $T_a = 1023 \text{ K}$ , there is no degradation of hard phase at an elevated temperature.

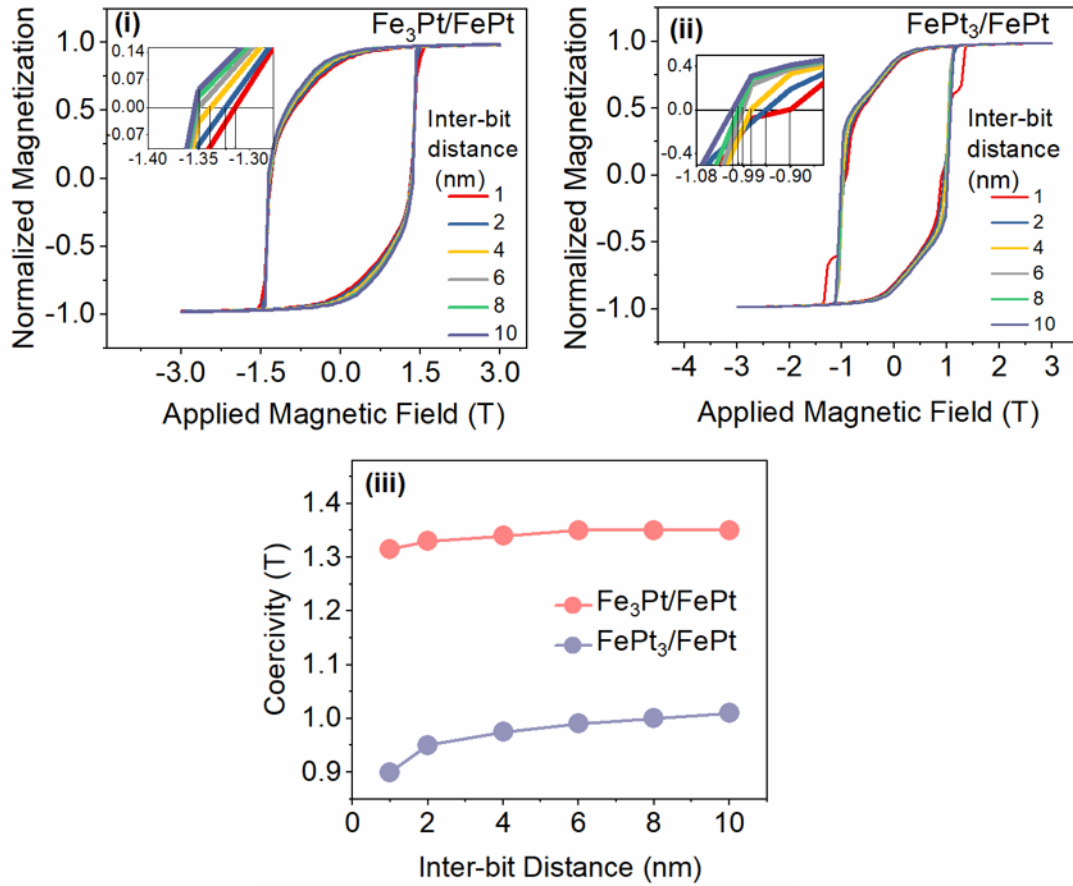


**Figure 7.** Simulated M-H curves by varying inter-bit distance from 1-10 nm for (i) Fe<sub>3</sub>Pt/FePt (ii) FePt<sub>3</sub>/FePt. Insets show the magnified image of hysteresis for obtaining coercivity values (iii) simulated coercivity as a function of inter-bit distance.

The values of  $K_{u1}$ (FePt) obtained from these coercivity comparisons are utilized further to investigate the effect of dipolar interaction. The dipolar interaction is studied by varying the inter-bit distance by increasing the total dimension of the system and fixing the 4×4 arrays of 12 nm bits. Figures 7(i) and (ii) respectively show the simulated M-H curves of Fe<sub>3</sub>Pt/FePt and FePt<sub>3</sub>/FePt as a function of inter-bit distance. Both, FePt<sub>3</sub>/FePt and Fe<sub>3</sub>Pt/FePt show a nominal inter-bit interaction effect i.e. almost constant coercivity values for large inter-bit distance from 4 to 10 nm and minimal increase in coercivity for 1-4 nm, as can be seen in Fig. 7(iii). The insets in Fig. 7(i)

and (ii) show the obtained coercivity values for comparing both layer schemes. In Fig.7 (i), the M-H curves for FePt<sub>3</sub>/FePt system with 1 nm interparticle distance shows a clear step that corresponds to the late reversal of corner bits, which is not seen in other simulated hysteresis. The late reversal of corner bits in the case of the inter-bit distance of 1 nm for FePt<sub>3</sub>/FePt is due to an increase of the demagnetizing field in the overall system. When the system is modeled with a total thickness of 12 nm and 1 nm inter-bit distance, the system more or less behaves like a continuous film. Also, it implies that at least 2 nm inter-bit distance is necessary for properly modeling dimensions with cylinder-shaped bits. Nevertheless, the minimal increase of coercivity can be attributed to negligible dipolar interaction between the inter-bit separated by 2-4 nm carbonaceous overcoat, beneficial for HDMR application.

## Conclusion

Hexagonal closed packed self-organization of non-stoichiometric Fe<sub>60</sub>Pt<sub>40</sub> NPs has been successfully synthesized using the chemical co-reduction method. The structural investigation of Si/Fe<sub>60</sub>Pt<sub>40</sub> and Si/Pt/Fe<sub>60</sub>Pt<sub>40</sub> system as a function of annealing temperature clearly revealed the transformation from chemically disordered phase to chemically ordered phase at low annealing temperature as compared to a system with nearly equi-atomic composition. The addition of the Pt buffer layer stabilizes the *L*<sub>10</sub> phase due to stoichiometric compensation at higher annealing temperature. Hence, the Pt buffer layer not only promotes the phase transformation at low temperature and but also helps in retaining a high coercivity over a wide range of annealing temperatures. Micromagnetic simulations were performed and compared with Fe<sub>3</sub>Pt/FePt and FePt<sub>3</sub>/FePt with respect to magnetic anisotropy and dipolar coupling. The results presented in the manuscript demonstrate the low ordering temperature using self-organization of chemically ordered magnetic nanoparticles which is sustained at high temperatures for HDMR based high-

density recording media.

## **Acknowledgments**

Financial support from JSPS Grant-in-Aid (KAKENHI No. 18H01862, 18H05953) is also gratefully acknowledged. This work is partially supported by the Nippon Sheet Glass Foundation.

R.M., S.G. and R.S.R. would like to acknowledge research grants, MOE2017-T2-2-129, NRF-CRP21-2018-0003 and MOE2019-T2-1-058.

## **Conflict of interest declaration**

The authors declare that there is no conflict of interest.

## References

- (1) Vogler, C.; Abert, C.; Bruckner, F.; Suess, D.; Praetorius, D. Heat-Assisted Magnetic Recording of Bit-Patterned Media beyond 10 Tb/in<sup>2</sup>. *Appl. Phys. Lett.* **2016**, *108* (10), 102406. <https://doi.org/10.1063/1.4943629>.
- (2) Tipcharoen, W.; Warisarn, C.; Tongsojorn, D.; Karns, D.; Kovintavewat, P. Investigation of Writing Error in Staggered Heated-Dot Magnetic Recording Systems. *AIP Adv.* **2017**, *7* (5), 056511. <https://doi.org/10.1063/1.4977762>.
- (3) Medwal, R.; Gautam, S.; Gupta, S.; Chae, K. H.; Asokan, K.; Deen, G. R.; Rawat, R. S.; Katiyar, R. S.; Annapoorni, S. Self-Stabilized Carbon-L1<sub>0</sub> FePt Nanoparticles for Heated Dot Recording Media. *IEEE Magn. Lett.* **2018**, *9* (May), 1–5. <https://doi.org/10.1109/LMAG.2018.2840990>.
- (4) Albrecht, T. R.; Patel, K.; Ruiz, R.; Schabes, M. E.; Wan, L.; Weller, D.; Wu, T.-W.; Bedau, D.; Dobisz, E.; Gao, H.; Grobis, M.; Hellwig, O.; Kercher, D.; Lille, J.; Marinero, E. Bit Patterned Media at 1 Tdot/in<sup>2</sup> and Beyond. *IEEE Trans. Magn.* **2013**, *49* (2), 773–778. <https://doi.org/10.1109/TMAG.2012.2227303>.
- (5) Weller, D.; Parker, G.; Mosendz, O.; Lyberatos, A.; Mitin, D.; Safonova, N. Y.; Albrecht, M. Review Article: FePt Heat Assisted Magnetic Recording Media. *J. Vac. Sci. Technol. B, Nanotechnol. Microelectron. Mater. Process. Meas. Phenom.* **2016**, *34* (6), 060801. <https://doi.org/10.1116/1.4965980>.
- (6) Gilbert, D. A.; Liao, J.-W.; Kirby, B. J.; Winklhofer, M.; Lai, C.-H.; Liu, K. Magnetic Yoking and Tunable Interactions in FePt-Based Hard/Soft Bilayers. *Sci. Rep.* **2016**, *6* (1), 32842. <https://doi.org/10.1038/srep32842>.
- (7) Sun, S.; Murray, C. B.; Weller, D.; Folks, L.; Moser, A. Monodisperse FePt Nanoparticles

- and Ferromagnetic FePt Nanocrystal Superlattices. *Science* (80-. ). **2000**, 287 (5460), 1989–1992. <https://doi.org/10.1126/science.287.5460.1989>.
- (8) Chen, M.; Liu, J. P.; Sun, S. One-Step Synthesis of FePt Nanoparticles with Tunable Size. *J. Am. Chem. Soc.* **2004**, 126 (27), 8394–8395. <https://doi.org/10.1021/ja047648m>.
- (9) Gutfleisch, O.; Lyubina, J.; Müller, K. K.-H.; Schultz, L.; Gutfleisch, B. O.; Lyubina, J.; Müller, K. K.-H.; Schultz, L. FePt Hard Magnets. *Adv. Eng. Mater.* **2005**, 7 (4), 208–212. <https://doi.org/10.1002/adem.200400183>.
- (10) Perumal, A.; Takahashi, Y. K.; Hono, K. L10 FePt–C Nanogranular Perpendicular Anisotropy Films with Narrow Size Distribution. *Appl. Phys. Express* **2008**, 1 (10). <https://doi.org/10.1143/APEX.1.101301>.
- (11) Medwal, R.; Sehdev, N.; Govind; Annapoorni, S. Electronic States of Self Stabilized L10 FePt Alloy Nanoparticles. *Appl. Phys. A* **2012**, 109 (2), 403–408. <https://doi.org/10.1007/s00339-012-7080-6>.
- (12) Medwal, R.; Sehdev, N.; Ying, W.; Rawat, R. S.; Annapoorni, S. Dense-Plasma-Driven Ultrafast Formation of FePt Organization on Silicon Substrate. *Bull. Mater. Sci.* **2017**, 40 (1), 233–238. <https://doi.org/10.1007/s12034-017-1359-3>.
- (13) Thomson, T.; Lee, S. L.; Toney, M. F.; Dewhurst, C. D.; Ogrin, F. Y.; Oates, C. J.; Sun, S. Agglomeration and Sintering in Annealed FePt Nanoparticle Assemblies Studied by Small Angle Neutron Scattering and X-Ray Diffraction. *Phys. Rev. B* **2005**, 72 (6), 064441. <https://doi.org/10.1103/PhysRevB.72.064441>.
- (14) Yano, K.; Nandwana, V.; Poudyal, N.; Rong, C.; Liu, J. P. Rapid Thermal Annealing of FePt Nanoparticles. *J. Appl. Phys.* **2008**, 104 (1), 013918. <https://doi.org/10.1063/1.2953078>.

- (15) Medwal, R.; Sehdev, N.; Annapoorni, S. Order–Disorder Investigation of Hard Magnetic Nanostructured FePt Alloy. *J. Phys. D. Appl. Phys.* **2012**, *45* (5), 055001. <https://doi.org/10.1088/0022-3727/45/5/055001>.
- (16) Pei, W.; Zhao, D.; Wu, C.; Sun, Z.; Liu, C.; Wang, X.; Zheng, J.; Yan, M.; Wang, J.; Wang, Q. Direct Synthesis of L10-FePt Nanoparticles with High Coercivity via Pb Addition for Applications in Permanent Magnets and Catalysts. *ACS Appl. Nano Mater.* **2020**, *3* (2), 1098–1103. <https://doi.org/10.1021/acsnm.9b02420>.
- (17) Abel, F. M.; Tzitzios, V.; Devlin, E.; Alhassan, S.; Sellmyer, D. J.; Hadjipanayis, G. C. Enhancing the Ordering and Coercivity of L10 FePt Nanostructures with Bismuth Additives for Applications Ranging from Permanent Magnets to Catalysts. *ACS Appl. Nano Mater.* **2019**, *2* (5), 3146–3153. <https://doi.org/10.1021/acsnm.9b00463>.
- (18) Liang, S.; Wang, F.; Zhang, Z.; Li, Y.; Cai, Y.; Ren, J.; Jiang, X. Monodisperse FePt Nanoparticles as Highly Active Electrocatalysts for Methanol Oxidation. *RSC Adv.* **2015**, *5* (60), 48569–48573. <https://doi.org/10.1039/c5ra07931d>.
- (19) Chen, J. S.; Xu, Y.; Wang, J. P. Effect of Pt Buffer Layer on Structural and Magnetic Properties of FePt Thin Films. *J. Appl. Phys.* **2003**, *93* (3), 1661–1665. <https://doi.org/10.1063/1.1531817>.
- (20) Seki, T.; Shima, T.; Takanashi, K.; Takahashi, Y.; Matsubara, E.; Hono, K. L10 Ordering of Off-Stoichiometric FePt (001) Thin Films at Reduced Temperature. *Appl. Phys. Lett.* **2003**, *82* (15), 2461–2463. <https://doi.org/10.1063/1.1567053>.
- (21) Gupta, R.; Medwal, R.; Annapoorni, S. Phase Investigation in Pt Supported Off-Stoichiometric Iron-Platinum Thin Films. *Mater. Res. Bull.* **2013**, *48* (10), 3881–3886. <https://doi.org/10.1016/j.materresbull.2013.05.119>.

- (22) Gupta, R.; Medwal, R.; Sharma, P.; Mahapatro, A. K.; Annapoorni, S. Effect of Pt Layers on Chemical Ordering in FePt Thin Films. *Superlattices Microstruct.* **2013**, *64*, 408–417. <https://doi.org/10.1016/j.spmi.2013.10.006>.
- (23) Gupta, R.; Medwal, R.; Sehdev, N.; Annapoorni, S. Pt Diffusion Driven  $L1_0$  Ordering in Off-Stoichiometric FePt Thin Films. *J. Magn. Magn. Mater.* **2013**, *345*, 60–64. <https://doi.org/10.1016/j.jmmm.2013.06.023>.
- (24) Medwal, R.; Gogia, K.; Thakar, D.; Vibhu, V.; Mohan, J. R.; Sehdev, N.; Annapoorni, S. Effect of Functionalization on Positional Ordering of 3 Nm FePt Nanoparticles: Langmuir–Blodgett Monolayer. *Surf. Coatings Technol.* **2014**, *258*, 509–514. <https://doi.org/10.1016/j.surfcoat.2014.08.048>.
- (25) Perumal, A.; Takahashi, Y. K.; Hono, K. Fe-Ta-C Soft Underlayer for Double-Layered Perpendicular Recording Media. *J. Appl. Phys.* **2009**, *105* (7), 10–13. <https://doi.org/10.1063/1.3058613>.
- (26) Takahashi, Y. K.; Seki, T. O.; Hono, K.; Shima, T.; Takanashi, K. Microstructure and Magnetic Properties of FePt and Fe/FePt Polycrystalline Films with High Coercivity. *J. Appl. Phys.* **2004**, *96* (1), 475–481. <https://doi.org/10.1063/1.1756688>.
- (27) Alexandrakis, V.; Niarchos, D.; Mergia, K.; Lee, J.; Fidler, J.; Panagiotopoulos, I. Magnetic Properties of Graded  $A1/L1_0$  Films Obtained by Heat Treatment of FePt/CoPt Multilayers. *J. Appl. Phys.* **2010**, *107* (1), 0–4. <https://doi.org/10.1063/1.3275925>.
- (28) Goll, D.; Breitling, A. Coercivity of Ledge-Type  $L1_0$ -FePt/Fe Nanocomposites with Perpendicular Magnetization. *Appl. Phys. Lett.* **2009**, *94* (5). <https://doi.org/10.1063/1.3078286>.
- (29) Dutta, T.; Piramanayagam, S. N.; Saifullah, M. S. M.; Bhatia, C. S. High Switching

- Efficiency in FePt Exchange Coupled Composite Media Mediated by MgO Exchange Control Layers. *Appl. Phys. Lett.* **2017**, *111* (4). <https://doi.org/10.1063/1.4996366>.
- (30) Dutta, T.; Piramanayagam, S. N.; Ru, T. H.; Saifullah, M. S. M.; Bhatia, C. S.; Yang, H. Exchange Coupled CoPt/FePtC Media for Heat Assisted Magnetic Recording. *Appl. Phys. Lett.* **2018**, *112* (14). <https://doi.org/10.1063/1.5012815>.
- (31) Hono, K.; Takahashi, Y. K.; Ju, G.; Thiele, J. U.; Ajan, A.; Yang, X. M.; Ruiz, R.; Wan, L. Heat-Assisted Magnetic Recording Media Materials. *MRS Bull.* **2018**, *43* (2), 93–99. <https://doi.org/10.1557/mrs.2018.5>.
- (32) Rong, C.-B.; Li, Y.; Liu, J. P. Curie Temperatures of Annealed FePt Nanoparticle Systems. *J. Appl. Phys.* **2007**, *101* (9), 09K505. <https://doi.org/10.1063/1.2709739>.
- (33) Medwal, R.; Sehdev, N.; Annapoorni, S. Temperature-Dependent Magnetic and Structural Ordering of Self-Assembled Magnetic Array of FePt Nanoparticles. *J. Nanoparticle Res.* **2013**, *15* (2), 1423. <https://doi.org/10.1007/s11051-013-1423-x>.
- (34) Suess, D.; Lee, J.; Fidler, J.; Schrefl, T. Exchange-Coupled Perpendicular Media. *J. Magn. Magn. Mater.* **2009**, *321* (6), 545–554. <https://doi.org/10.1016/j.jmmm.2008.06.041>.
- (35) Lyubina, J.; Opahle, I.; Müller, K.-H.; Gutfleisch, O.; Richter, M.; Wolf, M.; Schultz, L. Magnetocrystalline Anisotropy in L10 FePt and Exchange Coupling in FePt/Fe<sub>3</sub>Pt Nanocomposites. *J. Phys. Condens. Matter* **2005**, *17* (26), 4157–4170. <https://doi.org/10.1088/0953-8984/17/26/014>.
- (36) Rui, X.; Shield, J. E.; Sun, Z.; Skomski, R.; Xu, Y.; Sellmyer, D. J.; Kramer, M. J.; Wu, Y. Q. Intra-Cluster Exchange-Coupled High-Performance Permanent Magnets. *J. Magn. Magn. Mater.* **2008**, *320* (21), 2576–2583. <https://doi.org/10.1016/j.jmmm.2008.03.042>.
- (37) Zhang, J.; Liu, Y.; Wang, F.; Zhang, J.; Zhang, R.; Wang, Z.; Xu, X. Design and

Micromagnetic Simulation of the L10 -FePt/Fe Multilayer Graded Film. *J. Appl. Phys.*  
**2012**, *111* (7), 073910. <https://doi.org/10.1063/1.3702876>.

## Table of content

